A new device for the combined measurement of friction and through-thickness deformation on ex vivo skin samples

Bastien Eydan, Baptiste Pierrat, Nicolas Curt, Hassan Zahouani, Jérôme Molimard

A new device for the combined measurement of friction and through-thickness deformation on *ex vivo* skin samples

B.Eydan[1,*], B.Pierrat[1], N.Curt[1], H.Zahouani[2], J.Molimard[1].

[1] *Mines Saint-Etienne, Univ Lyon, Univ Jean Monnet, Etablissement Francais du Sang, INSERM, U 1059 Sainbiose, Centre CIS, F - 42023 Saint-Etienne France*
[2] *UMR 5513 Laboratoire de Tribologie et Dynamique des Systèmes, Université de Lyon - École Centrale de Lyon - École Nationale d'Ingénieurs de Saint-Étienne, France*

Abstract

Skin irritation is a common phenomenon that becomes a real concern when caused by the use of medical devices. Because the materials used for the design of these devices are usually carefully selected for chemical compatibility with the skin, it is reasonable to assume that the irritations result from the mechanical interaction between the devices and the skin. The aim of this work was to develop a new device to study both the shear strains in the layers of the skin, using Digital Image Correlation (DIC), and the friction behaviour of *ex vivo* skin interacting with objects. Pig skin samples with various surface preparations were tested in friction experiments involving different contacting materials encountered in the conception of medical devices. The measure of the static and dynamic coefficients of friction as well as the length of adhesion has highlighted the great influence of skin surface conditioning on friction properties. Strain maps obtained through DIC provided insights into the impact of friction and adhesion effects on shear strain distribution in the skin as a function of depth beneath its surface.

Keywords: Skin, Digital image correlation, Biotribology

1 Introduction

Skin is a multi-layered soft tissue that covers almost the entire body and is therefore the first to be exposed to objects. In addition to providing mechanical protection for other organs [1, 2], the skin helps in regulating body temperature, in particular thanks to a network of blood vessels located in the dermis [2–4]. The most external layer of skin, the stratum corneum, has a key role in the regulation of water transfer and acts as a barrier against biological contamination [2, 5]. Skin is also a very sensitive organ with millions of nerve receptors spread in the dermis and epidermis layers. In addition to mechanical receptors responsible for touch and pressure sensations, temperature and pain receptors [6] are responsible for warning the body of uncomfortable sensations felt when in contact with objects. For all these reasons, maintaining the physical integrity of the skin is essential.

Unfortunately, skin irritation is a common phenomenon that becomes a concern when caused by the use of medical devices. Physiologically, skin irritation can result in erythema, phlyctenes or swelling in addition to unpleasant sensations (heat, tingling, itching, dry skin) [7]. These are due to the stimulation of nociceptors located around the dermal-epidermal junction [8, 9]. Cutaneous irritations are for example an important issue for people who need a limb prosthesis [10]. The problem is also significant for people using compression textiles for the treatment or prevention of venous insufficiency. Indeed, many people find these devices very uncomfortable. Too many of them cannot bear to wear them to the point of abandoning their treatment [11].

Although they are common sources of skin irritation, exposure to a chemical agent or an allergic reaction [12] are unlikely to occur here as these medical devices are designed to be hypoallergenic. Cutaneous irritations can also be caused by the mechanical interaction of skin with objects: structurally, mechanical skin irritation usually means skin damage and the various studies on the subject agree that mechanical irritations are generally caused by prolonged or repeated contact with objects used on a daily basis [13]. The fact that a prolonged pressure can trigger the destruction of tissue cells leading to pressure ulcers, either through direct apoptosis or ischeamia, is now widely recognized [14, 15]. Goldstein and Sanders [16] showed how adding shear strain to pressure could accelerate and aggravate skin damaging. In addition several researches have demonstrated how friction is involved in the process of skin abrasion by progressively delaminating the cells of the stratum corneum [17]. The work of Naylor also concluded that blistering, for which shear strain is a determining factor, occurs at the base of the epidermal layer

*Corresponding author: B.Eydan,
E-mail: bastien.eydan@emse.fr

[18, 19]. Thus, mechanical irritation of the skin can take different forms, most likely to be induced by various mechanical stresses. It is reasonable to assume that these are partly determined by the properties of the interaction of the skin with objects.

The coefficient of friction is the most widely used metric to characterise the interaction of an object with the skin. Through a clinical study on the damage caused by repetitive rubbing of tissues on the skin, Thieulin et al. [17] showed how an increase in the coefficient of friction led to more pronounced symptoms of skin irritation. However, the numerous tests carried out to date have highlighted the influence of many factors on this coefficient [20]. Some depend on the properties of the contact material such as roughness and Young's modulus [21, 22]. Others are directly related to skin morphology and mechanical behaviour. Zahouani et al. [23] showed, for example, that friction forces increased for softer and smoother skins. This can be partly explained by an increase in contact area which leads to higher adhesion forces. A decrease in skin elasticity also tends to increase the friction forces due to the viscoelastic loss caused by the deformation of skin [24]. In addition, a numerical work by Leyva Mendivil et al. [25] showed how roughness could influence local friction properties, thus influencing stress propagation through skin layers. Finally, the environmental conditions in which contact takes place also play a considerable part. Indeed, it has been shown that local temperature and humidity influence the mechanical behaviour of the skin. This is notably linked to variations in skin hydration, in particular for the stratum corneum that is softened by increasing hydration [26–28]. Moreover, adhesion properties can also be modified by local micro-climate variations that will influence the nature of the hydro-lipidic layer covering skin. Furthermore, the application of products to the skin surface can also modify this interaction for the same reasons [29]. Because of the many parameters involved in measuring the coefficient of friction, and the interactions that exist between these parameters, it is impossible to generalize skin frictional behaviour. Hence, it is necessary to study each case as closely as possible to the real conditions.

The coefficient of friction alone does not allow to fully describe the mechanics involved in skin interaction with objects, as it integrates various local phenomena that are not generally uniform over the apparent area of contact. For example, using an optical method called digital image correlation (DIC), Liu et al. [30] showed that upon sliding contact with glass, the strains were not evenly distributed over the fingerpad. Despite OCT imaging of the skin epidermis while sliding, only a limited structural analysis in skin depth was possible. Other phenomena like stick-slip cannot be described by the coefficient of friction [24, 31, 32]. More, even though the complexity of the mechanical behaviour of the skin is widely recognized, most of the current literature on skin tribology is based on surface measurements and observations. An analysis of the deformations undergone by the skin in the through-thickness direction during contact could provide new insights into the phenomenon of mechanical irritation. Especially considering the variety of mechanical phenomena that can cause skin irritation, and the fact that they involve skin features lying beneath the surface.

The aim of this work was to develop a new device to study both the through-layer deformations and the friction behaviour of *ex vivo* skin interacting with objects. The analysis of the through-layer deformations is based on 2D DIC. This method allows to compute strains on the surface of a deforming sample by comparing groups of pixels between a reference image and images of the sample in a deformed state. It has already been used on skin, mainly on its surface in order to study skin wrinkling [33], tension properties [34, 35], surface strains due to contact [30], or to identify mechanical properties [36]. To our knowledge, the method has been applied in skin thickness only during oscillatory pure shear experiments [37, 38] that demonstrated the inhomogeneous and viscoelastic mechanical behaviour of the skin. The aim of this application to friction experiments was to relate the contact properties to the strains experienced in the skin thickness. This paper will first introduce the in-house measurement bench and the associated software that were designed specifically for the measurement of skin friction and deformations during contact. Then, a validation of the ability of the method to perform suitable friction measurements and to capture full-field through-thickness deformations of the skin using DIC will be developed. Finally, examples of friction and deformation measurements on pig skin samples will be described. The effect of skin surface preparation and the choice of contact material will be discussed regarding the case of compression stockings.

2 Material and methods

2.1 Measurement bench

A measurement bench was designed in-house with the purpose of measuring full-field through-thickness deformation along with frictional properties of skin strips in contact with a cylindrical probe (Figure 1). The probe axis is parallel to the sample top surface and normal to the imaging plane and the direction of travel in friction experiments. The principle of the measurement was to acquire pictures of the side of the sample with a camera during its interaction with the probe. Deformations were later computed using DIC using the open source Matlab software Ncorr [39].

The skin sample was held in the centre of the device by a system that allowed it to be stretched. The top, front and back surfaces of the samples were free, the bottom surface rested on the device and the side ones were used to apply tension in the sample. The device is designed

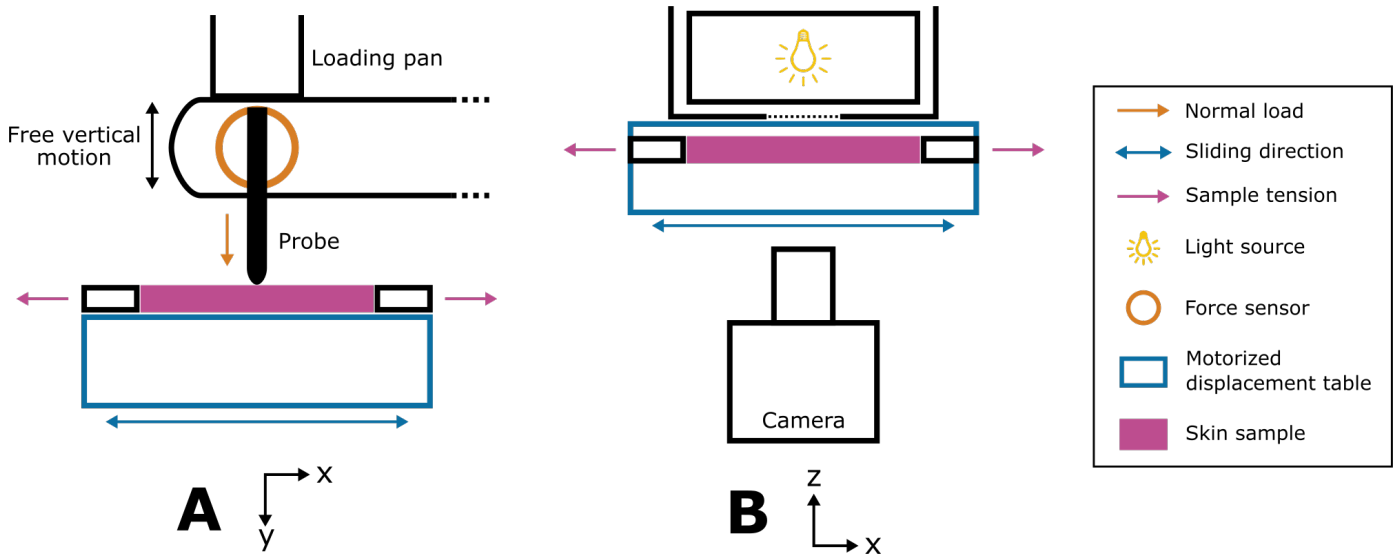

Figure 1: Schematic representation of the designed measurement bench. A: loading principle explained from the camera point of view. B: image acquisition principle explained from the top of the measurement bench.

in order to ensure that the side of the sample, of which images are made, is parallel to the imaging plane. The system used to hold the samples was mounted on a motorised displacement table (Thorlab, MTS25-Z8, Newton, NJ, USA) in order to control sliding of the sample against the cylindrical probe that was fixed in the horizontal plane but free in the vertical direction. The maximum sliding stroke, velocity and acceleration achievable by the displacement table were respectively $25mm$, $2.4mm.s^{-1}$ and $4.5mm.s^{-2}$. The probe was directly screwed on a 6-axis force sensor (K6D27 50N/1Nm, ME-Meßsysteme GmbH, Hennigsdorf, Germany), with a $50\mu N - 50N$ force measurement range and a 0.5% relative repeatability error. Normal load was applied using a deadweight in order to allow constant loading during friction testing without implementing a feedback loop. For that purpose, the force sensor was fixed at the extremity of a steel arm that freely rotates around its middle point, and on top of which two pans are fixed at each extremity to adjust the load. The pan at the opposite of the sensor helped equilibrating for the probe, sensor and arm weights while the second pan was used to effectively adjust the applied normal load with steel balls. The arm holding the probe and sensor was mounted on moving tables in order to adjust the probe position vertically and in both horizontal directions.

The camera (DMK 41BU02.H, 1280 × 980, The Imaging Source, Bremen, Germany) was positioned in front of the face of the sample, normal to its surface, on which the deformation will be calculated. It was fixed on moving tables that enable adjusting the focus and the field of view. The camera was equipped with a manual zoom lens (MLH-10X, CBC America, Cary, North Caroline, USA), and a 40mm lens extension tube. In this configuration, as the resolution of the camera was 1260x980 pixels, the width of 1 pixel was approximately 6µm, giving a total field of view of $7.56mm \times 5.88mm$. A light source using LED (MultiLED QT, GS Vitec, Gründau, Germany), which power was adjustable using an external control table (MultiLED G8, GS Vitec, Gründau, Germany), was located on the other side of the sample, allowing it to be back lit. A preliminary study has determined that if the samples are more than 4mm wide, the light does not pass through them sufficiently to have a good image quality.

The force sensor, the motorized displacement table and the camera were connected to a computer. A LabView program was created in order to coordinate all the devices of the bench and ensure good controlling of the acquisition process. It made it possible to adjust parameters of the displacement table (velocity, acceleration, and sliding stroke), the frequency of the image, displacement and load acquisition, to tare the force and to manually start and stop an experiment. The program displayed the current image and load or displacement curves in order to ensure the smooth running of the experiment. Load and displacement measures were synchronised and the acquisition frequency was set to 200Hz. The image acquisition rate was set to 10Hz, which was the maximum achievable frequency. All acquisitions were time-stamped.

2.2 Digital image correlation

As mentioned earlier, DIC is an optical method used to measure full-field displacements in samples undergoing deformation without touching them, thus without affecting the results. The correlation algorithm calculates the displacement of the points of the sample between its reference and deformed states by comparing the two corresponding images by subsets of pixels. The surface of the

sample must therefore exhibit a speckle pattern so that the correlation algorithm can find the transformation of each subset of pixels.

Usually, the algorithm gets an initial guess of the displacements of the points within the first analysed subset using fast normalized cross correlation [40]. Then, the transformation of this subset of the image is calculated through an iterative nonlinear least squares optimization such as the Gauss-Newton method [41]. A subpixel precision can be reached using a biquintic b-spline interpolation [42]. The process is repeated on the following subset; this time, the previously obtained information at the neighbouring subset is used as initial guess.

Before calculating strains the displacement field needs to be smoothed in order to remove as much noise as possible. Indeed, strain field computation is achieved by differentiation of the displacement field, which is very sensitive to high frequency variations. The first possible method to do that is to directly apply a lowpass filter on the displacement gradient obtained during the Gauss-Newton optimization [43, 44]. Another possibility is to first perform a least squares fit on a window of displacement points to obtain a smoothed field of displacement over that window and in a second step, calculate the displacement gradients [45]. Further details on the theory and algorithms of digital image correlation are available in the literature [46, 47].

2.3 Sample preparation

The 24 skin strip samples used hereby were 55mm long, 4mm wide and approximately 3mm thick, punched from the abdominal skin of the same female pig that was between 90 and 100 days old. As pictures of the skin section in its natural aspect did not provide a speckle pattern for DIC to be performed, samples were stained using hemalun and eosin [48, 49]. A preliminary study helped deciding the best combination of immersion time in both chemicals to get an optimal speckle pattern. Thus, the samples were first immersed for 30 seconds in the hemalun solution and immediately rinsed with water. They were then plunged for 10 seconds in the eosin solution and rinsed again with water. Both hemalun and eosin solutions were dilutions of the commercially available solutions. An example of the result of the staining step is shown in Figure 2.

After the staining, a 3D printed piece of plastic with a threaded hole was glued at either end of the sample. These pieces enabled attaching and aligning the samples on the measurement bench. It also enabled putting tension along the length of the samples using screws. Between each step of the preparation, samples were stored at 4°C in individual bags. Each sample was taken out of the fridge to be prepared just before starting the tests. A total of 24 samples were tested with three surface preparations to simulate different skin surface conditions. Eight were taken untreated to mimic natural skin with its lipidic layer. Eight were cleaned with liquid soap to remove the hydro-lipidic layer and approximate the skin just after a shower. The last eight were cleaned with liquid soap and then 15 tape stripping were applied to remove some of the stratum corneum and simulate mild irritation. All of the 24 samples were tested against the three different materials of contact. Using the tensioning screws of the device the tension within the samples was set to 10%, which is in the range of physiological skin stretching [34]. All the samples were processed within 48h after collecting them from the local butchery.

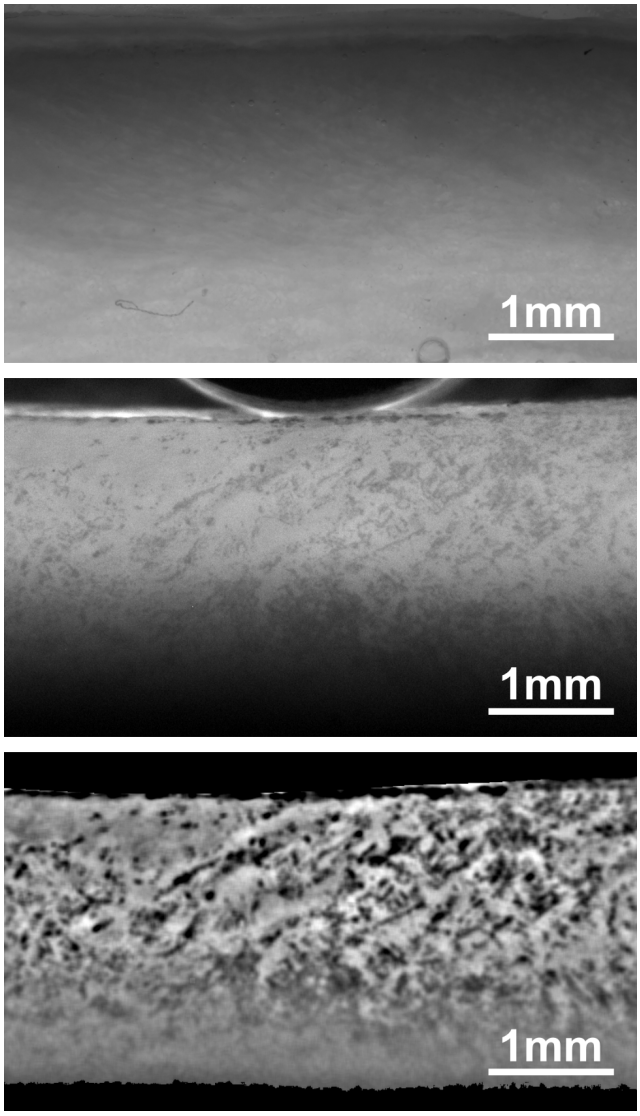

Figure 2: Photograph of the side of the skin sample in its natural aspect (top), after staining (middle) and after applying a high-pass filter (bottom). Here, the skin top surface is the top edge of the sample.

2.4 Validation of the method

The ability of this device to measure friction was assessed by performing cyclic friction experiments. The cylindrical probe surface was either stainless steel or sili-

cone and the counter-surface was made of stainless steel. This choice was made in order to be able to compare the results obtained with observations available in the literature. The sliding stroke was 4mm and the tests were performed with velocities of $0.1mm.s^{-1}$, $0.2mm.s^{-1}$, $0.5mm.s^{-1}$, $1.0mm.s^{-1}$ and $2.0mm.s^{-1}$. The experiment was repeated with normal loads of $0.25N$, $0.5N$, $1N$ and $2N$. A variety of sliding velocities and normal loads were used to verify the behaviour previously observed in other works for the friction of such materials. For every test, eight cycles were recorded in order to avoid preconditioning hysteresis if present. Finally the static coefficient of friction was calculated on the last 5 cycles as the ratio of tangential force to normal force when slipping began at the skin-probe interface.

The quality of the DIC measurements was evaluated through DIC calculation on pairs of images of 8 skin samples taken in the same position. The strains and measurement noise for the displacement calculation were expected to be zero since no loading is applied [50]. Thus, the standard deviation of the calculated displacements is representative of the overall quality achieved by the designed method. The size of the subset used in the analysis is a critical parameter. On one hand, it needs to be large enough so that every subset can be distinguished from each other due to unique grey-level distribution. But on the other hand, using a bigger subset would lead to increased approximations for the strain calculation step, especially with increasing level of deformations [46]. The minimum subset radius that should be taken in order to minimize the error can be identified by repeating the DIC on the couples of images with different subset sizes. Here the calculation were performed with a subset size varying between 20px and 100px. The effect of camera distortion was measured and was small enough to be considered as measurement noise. Similarly, an evaluation of out-of-plane deformations was carried out, and confirmed their negligible effect on the DIC measurements.

2.5 Measurement protocol

The skin samples were subjected to cyclic friction experiments with a 50g normal load. A 3mm sliding stroke was chosen to make sure that full sliding was reached. The sliding velocity was set to 0.2mm.s^{-1} in order to get sharp images despite the motion. The samples were subjected to 5 sliding cycles to ensure steady state sliding was reached. The experiment was repeated with three different contacting materials: the steel probe was covered with either a sheet of silicone rubber ($0.6mm$ thick) or textile ($0.5mm$ thick knitted polyamide) from a compression stocking, or used uncovered. Before each test the probe were gently cleaned with ethanol. In total, 72 experiments were carried out.

2.6 Signal processing

Only the last sliding cycle was considered for further analysis. The force sensor signals were low-pass filtered. Then the static coefficient of friction (μ_s) was taken as the first peak reached by the ratio of tangential force to normal force signal. The length of adhesion (L_{adh}) was taken as the sliding distance until this first peak was reached. Finally, the dynamic coefficient of friction (μ_d) was taken as the average of the ratio of tangential to normal force during steady state sliding. All these measures are summarized in figure 3, which shows a typical unidirectional sliding curve.

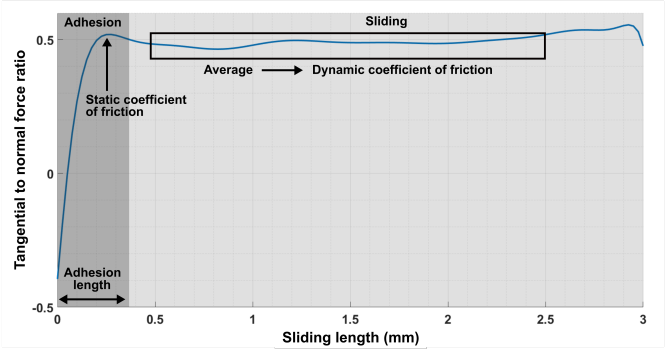

Figure 3: Example of how the coefficients of friction and adhesion length were measured using the force sensor signals.

2.7 Image processing

Before DIC can be applied, it was necessary to apply some filtering to the images. This last step aims to improve the contrast in order to enhance the speckle pattern quality. First, very high frequency noise was removed using a rectangular window filter. Then, the low frequencies were removed from the images in order to enhance the contours. The application of filters creates intermediate gray levels so this is why the images were converted into 16-bit gray level format to further improve the details. An example of image obtained after filtering is shown in figure 2.

The DIC was performed using the open source Matlab software Ncorr [39]. A preliminary experiment was carried out to determine the optimal size for subset radius. For all 72 experiments, the reference situation was a picture of the unloaded sample. The first deformed state analysed was just after adding the normal load, before any sliding occurred. Then, within the fifth and last sliding cycle, pictures with a displacement increment of 0.1mm were analysed until 1mm sliding. A subset radius of 60px and a subset spacing of 5px were chosen for the analysis. Strain maps were obtained after performing a linear fit over subsets of points from the displacement fields (window radius = 7pts). At each deformation state, an average strain map was obtained for every experimental condition by repositioning the maps in relation to the primary con-

tact point. Samples for which there were outliers in their deformation maps were removed from the calculation of the mean map. These aberrations were the result of poor quality correlation in a part of the region of interest. At least 5 trials per experimental situation were taken to obtain these average maps.

3 Results

3.1 Validation of the method

3.1.1 Friction measurements against stainless steel

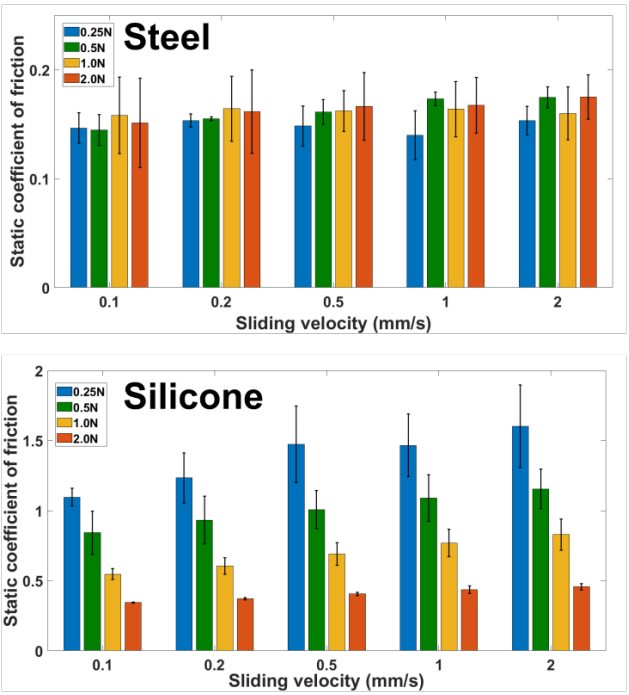

Figure 4: Static coefficient of friction (average ± standard deviation) of steel (top) and silicone (bottom) probe against steel with varying normal load and sliding velocity.

The resulting mean coefficients of friction tests against the stainless steel counter surface are presented in figure 4. Despite the variations in the sliding velocity and the normal load, the steel-to-steel coefficient of friction slightly fluctuated around 0.15 with a very low variability. This quasi-independence from the imposed contact conditions as well as the obtained coefficient of friction value are both in good agreement with the existing literature on steel-steel friction [51].

In contrast, the silicone-steel interaction exhibited a strong dependency to both the normal load and the sliding velocity. There was an increase of at least 32% and up to 52% in the coefficient of friction when the sliding velocity was increased from $0.1mm.s^{-1}$ to $2.0mm.s^{-1}$. This is in accordance with the theoretical model described by Li et al. [52]. They demonstrated a linear increase in the coefficient of friction of elastomers against steel when increasing the sliding velocity upto almost $10mm.s^{-1}$. Varying the normal load from 0.25N to 2.0N caused a decrease in the coefficient of friction of about 70%, for each of the velocities that were tested. Similar trends were observed in other work [53, 54], behaviour attributed to the viscoelastic deformation of the silicone.

3.1.2 Full-field displacements

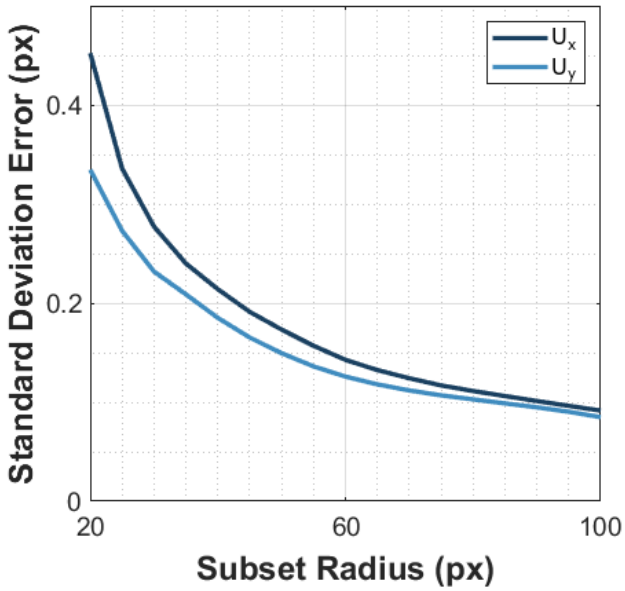

Figure 5: Average variation of the standard deviation on horizontal and vertical displacements calculated on pairs of images of skin samples in the same position using different subset sizes for the calculation of displacements.

In order to get a better idea of the accuracy of the DIC results obtained with this setup, the method has been applied to pairs of images taken in the same position with 8 samples. The resulting standard deviation on displacements should be zero and so any deviation from zero will reflect the overall experimental error [50]. The mean standard deviations obtained for horizontal (U_x) and vertical (U_y) displacements are plotted in figure 5. A fairly clear, albeit gradual, decrease in the slope of the curves is observed when increasing the subset radius. Most of the error is avoided when the slope variation is getting closer to zero. Using a much bigger size for the analysis will lead to an unwanted loss of spatial resolution, in addition to extending the computation time [55]. In the experiment presented here we can see that the slope is already getting much lower for a subset radius between 30px and 40px. This is in accordance with the sampling theorem of Nyquist-Shannon stating that the sampling rate should

be at least twice as high as the signal maximum frequency component in order to get a suitable reconstruction of the signal. Here the average speckle radius was 15.02±2.98px, leading to a minimal subset radius to consider in the range of 30px to 40px. Thus, we chose a slightly larger radius value of 60px, optimal even for cases with the largest average speckle sizes. With this subset size, the mean overall standard deviations due to the experimental conditions were 0.14±0.04px (i.e. 0.84±0.24µm) and 0.13±0.04px (i.e. 0.78±0.24µm) respectively for horizontal and vertical displacements.

The errors observed here are approximately one order of magnitude larger than the one observed by Avril et al. [56] with numerically applied displacements. However they are in the same range as the one obtained by Nguyen [57] who used the same method with synthetic materials. This level of random error can mainly be explained by the acquisition system and lighting conditions. Keeping constant light during the tests helped minimizing this random noise. The fact that skin is a living tissue that will creep and dry with time, can also lead to unwanted but real displacements and deformation.

3.2 Friction measurements against skin

All the measured indicators resulting from the processing of the force sensor signals from the last sliding cycles in each of the 72 experiments are summarized in table 1. Throughout these measurements, normal load was set to $50g$ and sliding velocity to $0.2mm.s^{-1}$. Both of the coefficients of friction and the adhesion length were higher for the silicone rubbed on cleaned and taped skin samples, and lower for the silicone against untreated skin.

The friction of the silicone on the skin was increased by a factor of 3.6 after cleaning and taping, the length of adhesion was increased by a factor of 5.4. However, the variability of the coefficients measured for the cleaned and taped samples was also greatly increased. By contrast, the values were slightly reduced by the skin surface preparation for measurements with the bare steel and the textile-covered probe. Though steel and textile gave similar coefficients of friction, the adhesion length obtained with the textile covered probe was about twice as high, regardless of the surface preparation.

Skin surface	Material	$\mu_s[-]$	$\mu_d[-]$	$L[mm]$
Untreated	Steel	0.40 ± 0.08	0.35 ± 0.07	0.19 ± 0.08
	Silicone	0.18 ± 0.06	0.17 ± 0.05	0.17 ± 0.05
	Textile	0.38 ± 0.05	0.38 ± 0.05	0.53 ± 0.16
Clean	Steel	0.33 ± 0.10	0.27 ± 0.08	0.19 ± 0.09
	Silicone	0.54 ± 0.21	0.51 ± 0.18	0.70 ± 0.31
	Textile	0.32 ± 0.10	0.30 ± 0.07	0.36 ± 0.13
Tape	Steel	0.34 ± 0.09	0.29 ± 0.10	0.20 ± 0.13
	Silicone	0.66 ± 0.20	0.64 ± 0.21	0.92 ± 0.30
	Textile	0.34 ± 0.07	0.33 ± 0.07	0.43 ± 0.22

Table 1: Average ± standard deviation of the static (μ_s) and dynamic (μ_d) coefficients of friction and adhesion length (L) calculated on the last sliding cycle for the 9 different experimental conditions.

Figure 6 shows the average curves of the ratio of tangential force to normal force for each situation. The different types of interactions obtained by varying the contact material and the skin surface condition can be appreciated. It can also be seen how little influence the skin surface preparation has on the interaction of the skin with the textile and steel probes.

3.3 Full-field strains

The shear strain maps show most explicitly the differences due to contact properties compared to the normal strain maps (ε_{xx} and ε_{yy}). This is why they are the only ones that will be described. Since the deformation was applied by the probe across the entire width of the sample, and based on other boundary conditions, an in-plane

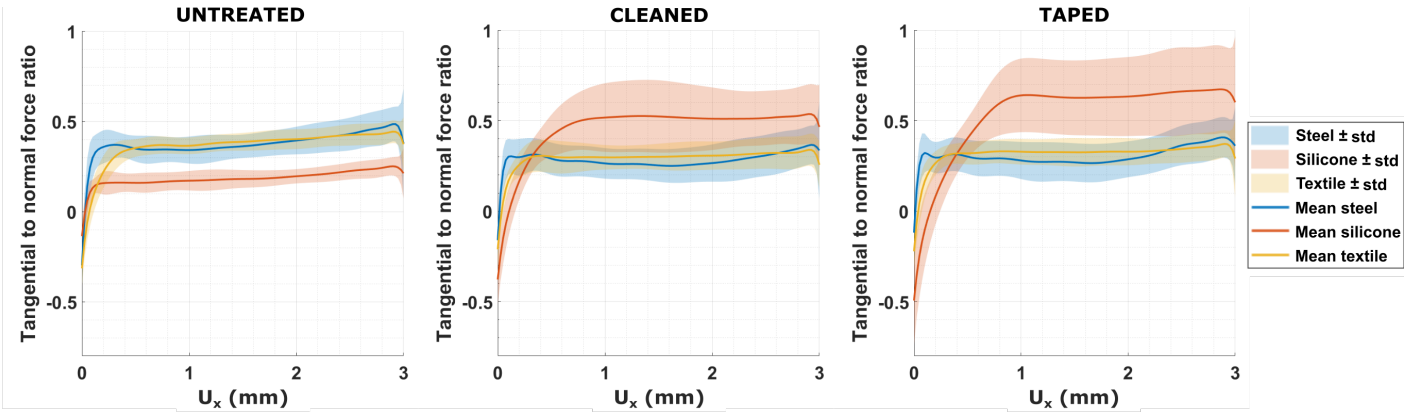

Figure 6: Evolution of the tangential to normal force ratio for the last sliding cycle in friction experiments on skin. Each curve and associated envelope gives mean and standard deviation values across the values obtained for the eight samples for a given combination of probe (steel, silicone or textile) and skin preparation (Untreated, cleaned or taped).

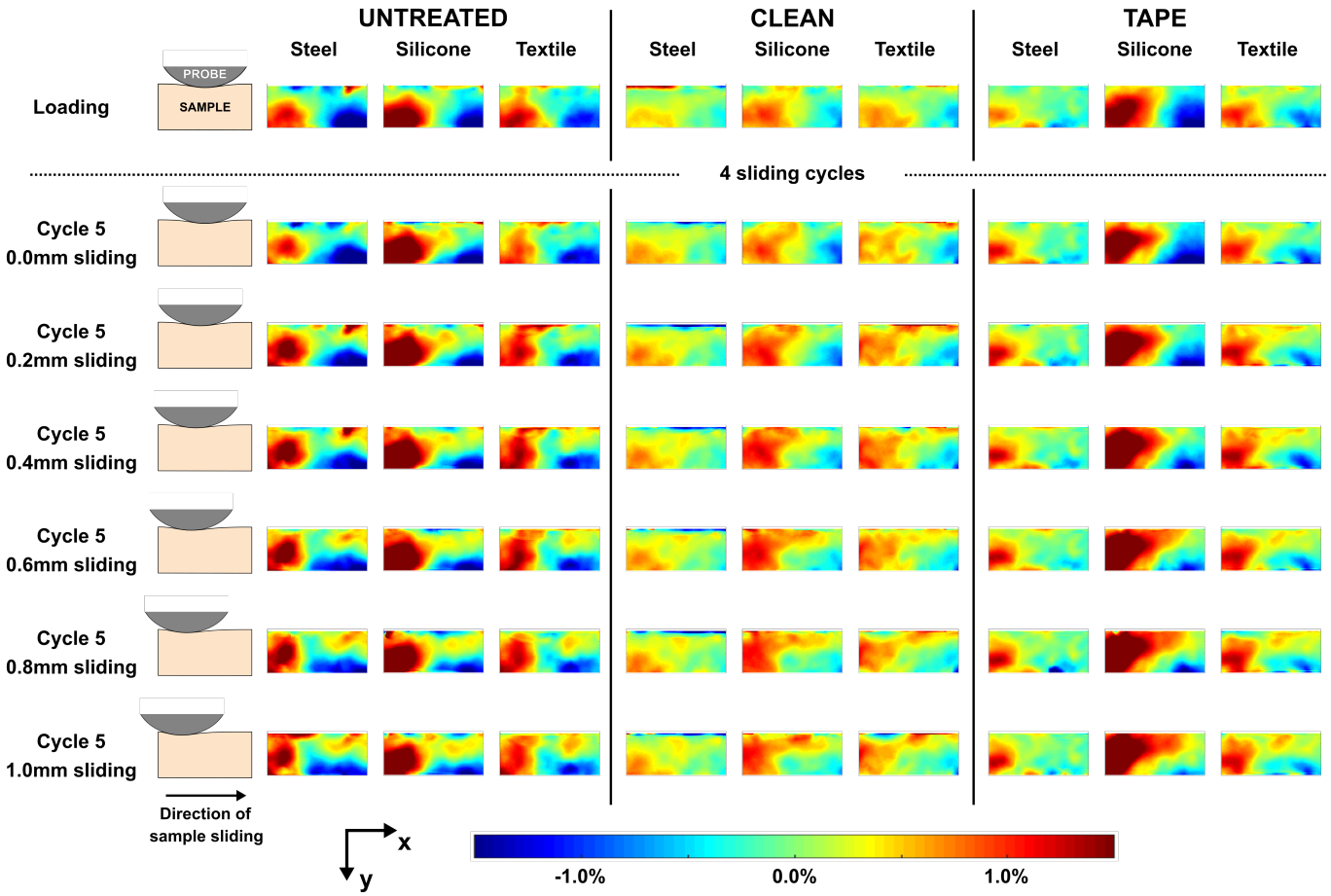

Figure 7: Average Green-Lagrange shear strain (γ_{xy}) maps obtained by the DIC processing. The rows show different time steps of the experiment while the column stand for the various skin surface preparation and material of contact. For each skin surface preparation 8 samples were tested using the three material of contact. These maps are obtained averaging over the 8 samples tested in each contact condition. The normal load was $50g$ and the sliding velocity $0.2mm.s{-}1$. Shear strain maps window are 4mm wide, centered on the initial point of contact. The top of all maps is $0.1mm$ beneath skin surface and the maps height is $1.65mm$.

stress configuration is assumed. As a consequence the deformation of the sample can be considered as almost homogeneous across its width. All of the average Green-Lagrangian shear strain maps for the loading and first millimeter sliding of the fifth sliding cycle are shown in figure 7. The maps displayed here are vertically centered on the initial line of contact. They show a 4mm wide window of the shear strain from 0.1mm to 1.75mm under the samples surface. This size of window has been chosen because for some of the samples the correlation was simply impossible or with too low quality very close to the top of skin surface. This could be explained by the fact that the compression was the highest in that area. Some lighting variations due to the movement of the probe and side effects may also come into play and affect the DIC in that area of the region of interest.

Some differences in the shapes of the contours can easily be seen between the different materials and surface preparation. In addition, their evolution during sliding also indicates different responses of the skin samples. Furthermore, it can be seen that the intensity of the deformations and their spread through the thickness of the skin samples as the sliding progresses are also influenced by the contact conditions. For example, with the steel on untreated skin, the intensity of the shear strain increasing until 0.2mm of sliding and then remains almost constant. With steel as a contacting material, the shape of shear contours remains very similar to the one just after adding normal load. This is also true with the silicone sliding on untreated skin. By contrast, for the silicone on both cleaned and taped skin, the shear strain spreads in the sample up to almost 1mm of sliding. This also seems to be the case for situations where the contact material is textile, although it is somewhat less obvious.

4 Discussion

The objective of this work was to develop a new method to simultaneously measure friction and through-thickness deformation of *ex vivo* skin samples. After validating the

method with basic experiments, it has been applied to study the influence of the contacting material and skin surface preparation on their frictional interaction.

4.1 The different friction mechanisms

The surface of the skin is covered by a fluid film that is resulting both from the degradation of keratinocytes in the epidermis and from the secretion of sebaceous glands. This hydro-lipidic layer mainly contain water, amino acids and sebum, and is a few micrometer thick depending on the body location [58]. In untreated skin, objects first come into contact with this fluid layer before solid-solid contact can occur. The friction properties are therefore mainly governed by the physico-chemical properties of this layer [59]. By modifying the surface condition of the skin, the aim was to recreate different friction conditions that patients might encounter when wearing compression devices. Cleaning was performed to partly remove the hydro-lipidic layer, thus modifying the surface energy of the skin [60].The application of tape-stripping was applied to rip out cells of the stratum corneum, softening skin surface [61]. In both cases, the mechanism of interaction between skin and the contacting objects probably evolved consequently.

The silicone-skin interaction was the most influenced by this change as μ_s, μ_d, and L_{adh} were substantially increased after cleaning and taping skin surface. Pailler-Mattei et al. [60] study of the skin surface physical properties concluded that the hydro-lipidic layer was responsible for most of the adhesive behaviour of the skin. They also observed that skin was more hydrophobic when removing this very thin film using ether. The silicone used in this study was hydrophobic, so the hydrolipid film most likely exerted repulsive forces on the silicone surface. Hence, removing this hydrophilic film would have modified the mechanism of interaction, leading to an increase in the area of contact between the probe and the skin. This could explain the significant increase in both coefficients of friction and adhesion length after cleaning. This is in line with the observations of Kékicheff [62] on hydrophobic surfaces interactions. This would also help to explain the increase in the adhesion length. As mentioned earlier the tape stripping was meant to soften the skin and reduce the roughness of the surface. Both effects would lead to an increase in the actual contact area, especially for a material such as silicone, whose roughness is negligible compared to the one of the skin. This would be sufficient to explain the additional increase in adhesion and coefficients of friction.

Steel, on the other hand, is hydrophilic and the hydrolipid film tends to create attractive forces by creating capillary bridges [59, 60], which may explain the slight decrease observed in the coefficients of friction after cleaning. Pailler-Mattei et al. [63] measured an increase by a factor 2 after tape-stripping for the coefficient of friction of a steel probe against skin. They explained this variation by an increase in the transepidermal water loss that would tend to increase the capillary forces. On the contrary, here the results were not affected by the tape-stripping. This different behaviour observed is probably due to the fact that the measurement were performed on *ex-vivo* samples, meaning they were not able to vary water flows. Another noticeable difference is the contact pressure that was 10 to 100 times higher in the present study. Such contact pressure may break the capillary bridges and compromise the increase of adhesion forces [59].

Textile friction and adhesion properties seem to evolve in the same way as with steel. However, these two materials have very different mechanical and roughness characteristics. Thus, interaction between the asperities of the two rough materials could be added to the usual physico-chemical interactions of surfaces. In the untreated skin condition, the coefficients of friction were similar to those for the steel. However, as the textile surface is much rougher, the real area of contact is reduced despite the elastic deformation of the textile asperities. It is therefore reasonable to assume that the hydro-lipidic layer creates strong adhesive forces with the textile fibres that compensate for this difference. Cleaning would tend to reduce the attraction between the skin surface and the textile, as opposed to the case of silicone. But the direct contact of the asperities of the two surfaces might cause an increase of the elastic deformation. This would explain why only a very low decrease of the friction properties is observed. Finally, the tape stripping did not influence the friction results with the textile.

4.2 Influence of the experimental conditions on the deformation fields

Before starting the analysis of the deformation patterns obtained by DIC for each experimental condition, a few technical aspects must be mentioned. Firstly, in order to minimise errors and uncertainties, the DIC analysis was carefully executed for all of the experiments and only results with good correlation were kept for the analysis. However, for a significant number of samples, it was difficult to obtain sufficient correlation quality in the first tenths of a millimetre below skin surface due to higher levels of deformation, variations in illumination, and probe movement. The same difficulty also happened close to the bottom support due to blurring. It should also be noted that different samples were used for each surface preparation. This choice was imposed by the duration of the experiment, which did not allow the tests to be carried out for the three surface preparations without the samples drying out. The intensity of the deformations measured depended greatly on the samples, even though they were all recovered from a single pig, in the same area of the skin and cut with the same orientation. This makes the quantitative measurements complicated but does not compromise the qualitative analysis of the strain contours.

Even though some adhesion phenomena can already occur just after the normal loading, the first stage analysed by DIC can be considered as a reference to analyse the different effects caused by the relative sliding of the surfaces. For each of the contact conditions, two shear lobes of opposite signs can be seen in the depth of the samples. This pattern, well centred on the contact point, is typical of the deformation caused by the indentation. Some variations in the intensity and spreading of the lobes can be observed and might be attributed to differences in the mechanical properties of the contacting objects as well as the adhesion between the two surfaces. The lobes created by the steel seem to be tighter and do not rise towards the sample surface. On the contrary, for textile and silicone the lobes are more spread out. For the silicone there is an increasing shear effect close to the samples surface when the surface is cleaned and then tape-stripped. Almost the opposite can be observed for textile. This could mean that the stronger the adhesion, the more the upper layers of the skin are sheared off.

During the sliding, the intensity of the shear strain is amplified. It would seem that this is all the more true when the frictional forces are high. This is indeed the case for steel and textile on untreated skin, as well as for silicone and textile on cleaned and tape stripped samples. On the contrary, no obvious evolution is to be noted for silicone on untreated skin and steel in cleaned and tape stripped situations, which confirms this first observation. In cases where adhesion forces were high, the shear tended to spread to the upper part of the sample as it moved. This is very pronounced for the silicone sliding on tape-stripped skin. In situations where both friction and adhesion were low, the maps stayed very similar to the one obtained immediately after normal load was applied. Adhesion seemed to ease the spread of shear strain, especially in the upper part of the skin. Frictional forces would be mainly responsible for the increase in shear intensity. Interestingly, the shear intensity did not seem to vary much once sliding between the two surfaces begins.

4.3 Perspectives

As stated in the introduction, the aim of this work was to develop a device to visualize strains through skin thickness during contact with objects. The final objective was to provide new elements for the understanding of skin irritation mechanisms. The designed method successfully allowed to study the deformation patterns in the first millimeters below skin samples surface during the sliding contact against various materials. This is also the first time that a combined analysis of the full-field strains through the skin thickness and the friction forces is performed. The data collected highlighted the non-uniformity of the deformations undergone by the skin during contact. The indicators that were measured in parallel made it possible to analyse the effects of friction and adhesion. The influence of the material of contact and the condition of the skin surface on the contact mechanism was thus emphasised. The first results obtained by this method pave the way for future work to better understand the tribology of the skin. These results could, for example, be used for the design of a numerical model allowing an in-depth analysis of the risk factors for the development of skin irritations.

For that purpose, it may be beneficial to modify the device so that the strains can be accurately visualised even within the epidermis and near the dermal-epidermal junction. It is indeed around this area of the skin that many nerve receptors sensitive to mechanical stimuli are located. Damage resulting from the repetitive rubbing of objects on the skin also occurs mainly in the immediate vicinity of the skin's surface.

Measuring the effects of the different surface preparation on skin surface chemical content, geometry and mechanical properties would greatly improve the analysis of skin contact properties. The work presented here has already shown that different skin surface conditions can significantly alter skin behaviour. However, the analysis of the results was based on a review of the literature which is still incomplete on this subject. In order to provide an even more correct analysis, it would also be interesting to study the influence of the staining step on the mechanical behaviour of the skin. In the same vein, controlling the humidity and temperature conditions could also add to the knowledge of the contact properties of the skin.

5 Conclusion

A new method has been developed to simultaneously measure the frictional behaviour and deformation through the thickness of skin samples. It was used here to study the influence of the skin surface condition and the contacting material on skin deformation and contact properties. Although improvements need to be made to increase the accuracy of DIC, particularly near the surface of the samples, the method has proven to be successful in studying the effects of contact properties on the strains undergone by skin in its thickness. Using different materials and surface preparation permitted to reach different friction and adhesion regimes. The analysis of the shear maps obtained under these different contact conditions allowed us to catch a glimpse of how they can influence the through-thickness deformation behaviour of the skin. In particular, adhesion seemed to influence the spreading of the shear strain close to the sample surface as shown by the strain maps resulting from the interaction of skin with the silicone rubber. Increasing coefficient of friction was found to be responsible for higher strain intensities. There was a great influence of the preparation of skin surface, this reinforced the idea that it is necessary to study each case as closely as possible to the real conditions. The application of this method under even more varied conditions may contribute to the understanding of the effects of contact on the skin. This could provide new insights for many

medical and industrial applications where skin comfort is an absolute necessity.

Credit author statement

B.Eydan: Conceptualization, Methodology, Validation, Formal analysis, Investigation, Writing - Original Draft.

J.Molimard: Conceptualization, Methodology, Software, Formal analysis, Writing - Review & Editing, Supervision, Funding acquisition.

B.Pierrat: Conceptualization, Methodology, Writing - Review & Editing.

N.Curt: Methodology.

H.Zahouani: Writing - Review & Editing.

Declaration of interests

The authors declare that they have no known competing financial interests or personal relationships that could have appeared to influence the work reported in this paper.

Acknowledgements

This study was supported by the Auvergne-Rhône-Alpes region through the "Pack Ambition Recherche" grant.

References

[1] Pierre Agache and Daniel Varchon. "46 skin mechanical function". In: Measuring the Skin. Publisher: Springer Science & Business Media Germany. Springer, 2004, pp. 429–445. ISBN: 3-540-01771-2.

[2] CB Archer. "Functions of the skin". In: Rook's textbook of dermatology. 7th ed. Vol. 1. Publisher: Wiley Online Library. Blackwell, 2010. ISBN: 0-632-06429-3.

[3] JA McGrath, RAJ Eady, and FM Pope. "Anatomy and organization of human skin". In: Rook's textbook of dermatology. Vol. 1. Publisher: Wiley-Blackwell, London, UK, 2010. ISBN: 0-632-06429-3.

[4] Pierre Agache. "33 Skin Blood Flow: Histophysiology". In: Measuring the Skin. Publisher: Springer Science & Business Media. Springer, 2004, pp. 329–335. ISBN: 3-540-01771-2.

[5] Jan D Bos and Martien L Kapsenberg. "The skin immune system: progress in cutaneous biology". In: Immunology today 14.2 (1993). Publisher: Elsevier, pp. 75–78. ISSN: 0167-5699. DOI: 10.1016/0167-5699(93)90062-P.

[6] Nicholas Boulais and Laurent Misery. "The epidermis: a sensory tissue". In: European Journal of Dermatology 18.2 (2008), pp. 119–127. ISSN: 1167-1122. DOI: 10.1684/ejd.2008.0348.

[7] Sara Weltfriend, Michal Ramon, and Howard I Maibach. "Irritant dermatitis". In: Dermatotoxicology, 2004. ISBN: 978-0-203-42627-2.

[8] David T Graham, Helen Goodell, and Harold G Wolff. "Neural mechanisms involved in itch,"itchy skin," and tickle sensations". In: The Journal of clinical investigation 30.1 (1951). Publisher: Am Soc Clin Investig, pp. 37–49. ISSN: 0021-9738. DOI: 10.1172/JCI102414.

[9] Martin Schmelz et al. "Specific C-receptors for itch in human skin". In: Journal of neuroscience 17.20 (1997). Publisher: Soc Neuroscience, pp. 8003–8008. ISSN: 0270-6474. DOI: 10.1523/JNEUROSCI.17-20-08003.1997.

[10] W Li et al. "Effect of prosthetic socks on the frictional properties of residual limb skin". In: Wear 271.11-12 (2011). Publisher: Elsevier, pp. 2804–2811. ISSN: 0043-1648. DOI: 10.1016/j.wear.2011.05.032.

[11] S Reich-Schupke et al. "Quality of life and patients' view of compression therapy". In: International angiology 28.5 (2009). Publisher: Edizioni Minerva Medica, p. 385. ISSN: 0392-9590.

[12] Thomas Welss, David A Basketter, and Klaus R Schröder. "In vitro skin irritation: facts and future. State of the art review of mechanisms and models". In: Toxicology in vitro 18.3 (2004). Publisher: Elsevier, pp. 231–243. ISSN: 0887-2333. DOI: 10.1016/j.tiv.2003.09.009.

[13] U Wollina. "Mechanical skin irritations due to textiles". In: Handbook of Medical Textiles. Elsevier, 2011, 248–268e. ISBN: 978-1-84569-691-7.

[14] Carlijn V Bouten et al. "The etiology of pressure ulcers: skin deep or muscle bound?" In: Archives of physical medicine and rehabilitation 84.4 (2003). Publisher: Elsevier, pp. 616–619. ISSN: 0003-9993. DOI: 10.1053/apmr.2003.50038.

[15] Parco M Siu et al. "Muscle apoptosis is induced in pressure-induced deep tissue injury". In: Journal of applied physiology 107.4 (2009). Publisher: American Physiological Society Bethesda, MD, pp. 1266–1275. ISSN: 8750-7587. DOI: 10.1152/japplphysiol.90897.2008.

[16] Barry Goldstein and Joan Sanders. "Skin response to repetitive mechanical stress: a new experimental model in pig". In: Archives of physical medicine and rehabilitation 79.3 (1998), pp. 265–272. ISSN: 0003-9993. DOI: 10.1016/S0003-9993(98)90005-3.

[17] C Thieulin et al. "Wear of the stratum corneum resulting from repeated friction with tissues". In: Wear 376 (2017), pp. 259–265. ISSN: 0043-1648. DOI: 10.1016/j.wear.2016.10.024.

[18] PFD Naylor. "Experimental friction blisters." In: British Journal of Dermatology 67.10 (1955). Publisher: Wiley Online Library, pp. 327–342. ISSN: 0007-0963. DOI: 10.1111/j.1365-2133.1955.

[19] Joseph J Knapik et al. "Friction blisters". In: Sports Medicine 20.3 (1995). Publisher: Springer, pp. 136–147. ISSN: 1179-2035. DOI: 10.2165/00007256-199520030-00002.

[20] S Derler and L-C Gerhardt. "Tribology of skin: review and analysis of experimental results for the friction coefficient of human skin". In: Tribology Letters 45.1 (2012), pp. 1–27. ISSN: 1023-8883. DOI: 10.1007/s11249-011-9854-y.

[21] Emile Van Der Heide, Xiangqiong Zeng, and Marc Arthur Masen. "Skin tribology: Science friction?" In: Friction 1.2 (2013). Publisher: Springer, pp. 130–142. ISSN: 2223-7690. DOI: 10.1007/s40544-013-0015-1.

[22] CP Hendriks and SE Franklin. "Influence of surface roughness, material and climate conditions on the friction of human skin". In: Tribology Letters 37.2 (2010). Publisher: Springer, pp. 361–373. ISSN: 1573-2711. DOI: 10.1007/s11249-009-9530-7.

[23] H Zahouani et al. "Effect of human ageing on skin rheology and tribology". In: Wear 271 (2011). Publisher: Elsevier, pp. 2364–2369. DOI: 10.1016/j.wear.2011.02.024.

[24] Michael J Adams, Brian J Briscoe, and Simon A Johnson. "Friction and lubrication of human skin". In: Tribology letters 26.3 (2007). Publisher: Springer, pp. 239–253. ISSN: 1573-2711. DOI: 10.1007/s11249-007-9206-0.

[25] Maria F Leyva-Mendivil et al. "Skin microstructure is a key contributor to its friction behaviour". In: Tribology Letters 65.1 (2017), p. 12. ISSN: 1023-8883. DOI: 10.1007/s11249-016-0794-4.

[26] Yonghui Yuan and Ritu Verma. "Measuring microelastic properties of stratum corneum". In: Colloids and Surfaces B: Biointerfaces 48.1 (2006). Publisher: Elsevier, pp. 6–12. ISSN: 0927-7765. DOI: 10.1016/j.colsurfb.2005.12.013.

[27] Richard H Wildnauer, James W Bothwell, and Alexander B Douglass. "Stratum corneum biomechanical properties I. Influence of relative humidity on normal and extracted human stratum corneum". In: Journal of Investigative Dermatology 56.1 (1971). Publisher: Elsevier, pp. 72–78. ISSN: 0022-202X. DOI: 10.1111/1523-1747.ep12292018.

[28] Kenneth S Wu, William W van Osdol, and Reinhold H Dauskardt. "Mechanical properties of human stratum corneum: effects of temperature, hydration, and chemical treatment". In: Biomaterials 27.5 (2006). Publisher: Elsevier, pp. 785–795. ISSN: 0142-9612. DOI: 10.1016/j.biomaterials.2005.06.019.

[29] Raja K Sivamani and HI Maibach. "Tribology of skin". In: Proceedings of the Institution of Mechanical Engine 220.8 (2006). Publisher: SAGE Publications Sage UK: London, England, pp. 729–737. ISSN: 1350-6501. DOI: 10.1243/13506501JET85.

[30] X Liu et al. "New Non-invasive Techniques to Quantify Skin Surface Strain and Sub-surface Layer Deformation of Finger-pad during Sliding". In: Biotribology 12 (2017), pp. 52–58. ISSN: 2352-5738. DOI: 10.1016/j.biotri.2017.07.001.

[31] S Derler and G-M Rotaru. "Stick–slip phenomena in the friction of human skin". In: Wear 301.1-2 (2013). Publisher: Elsevier, pp. 324–329. ISSN: 0043-1648. DOI: 10.1016/j.wear.2012.11.030.

[32] Emad Kamil Hussein, Kussay Ahmed Subhi, and Tayser Sumer Gaaz. "Effect of Stick-Slip Phenomena between Human Skin and UHMW Polyethylene." In: Pertanika Journal of Science & Technology 29.3 (2021). ISSN: 0128-7680. DOI: 10.47836/pjst.29.3.06.

[33] Nagisa Miura et al. "Digital image correlation strain analysis for the study of wrinkle formation on facial skin". In: Journal of Solid Mechanics and Materials Engineering 6.6 (2012). Publisher: The Japan Society of Mechanical Engineers, pp. 545–554. ISSN: 1880-9871. DOI: 10.1299/jmmp.6.545.

[34] Raman Maiti et al. "In vivo measurement of skin surface strain and sub-surface layer deformation induced by natural tissue stretching". In: journal of the mechanical behavior of biomedical materials 62 (2016), pp. 556–569. ISSN: 1751-6161. DOI: 10.1016/j.jmbbm.2016.05.035.

[35] E Guan et al. "Determining the mechanical properties of rat skin with digital image speckle correlation". In: Dermatology 208.2 (2004), pp. 112–119. ISSN: 1018-8665. DOI: 10.1159/000076483.

[36] Samuel Lewin Evans and Catherine Avril Holt. "Measuring the mechanical properties of human skin in vivo using digital image correlation and finite element modelling". In: The Journal of Strain Analysis for Engineering Design 44.5 (2009), pp. 337–345. ISSN: 0309-3247. DOI: 10.1243/03093247JSA488.

[37] L-C Gerhardt et al. "A novel method for visualising and quantifying through-plane skin layer deformations". In: Journal of the mechanical behavior of biomedical materials 14 (2012). Publisher: Elsevier, pp. 199–207. ISSN: 1751-6161. DOI: 10.1016/j.jmbbm.2012.05.014.

[38] E Lamers et al. "Large amplitude oscillatory shear properties of human skin". In: journal of the mechanical behavior of biomedical materials 28 (2013). Publisher: Elsevier, pp. 462–470. ISSN: 1751-6161. DOI: 10.1016/j.jmbbm.2013.01.024.

[39] J Blaber, B Adair, and A Antoniou. "Ncorr: open-source 2D digital image correlation matlab software". In: Experimental Mechanics 55.6 (2015). Publisher: Springer, pp. 1105–1122. ISSN: 0014-4851. DOI: 10.1007/s11340-015-0009-1.

[40] Shou-Der Wei and Shang-Hong Lai. "Fast template matching based on normalized cross correlation with adaptive multilevel winner update". In: IEEE Transactions on Image Processing 17.11 (2008). Publisher: IEEE, pp. 2227–2235. ISSN: 1057-7149. DOI: 10.1109/TIP.2008.2004615.

[41] B Pan, K Li, and W Tong. "Fast, robust and accurate digital image correlation calculation without redundant computations". In: Experimental Mechanics 53.7 (2013). Publisher: Springer, pp. 1277–1289. ISSN: 0014-4851. DOI: 10.1007/s11340-013-9717-6.

[42] Hubert W Schreier, Joachim R Braasch, and Michael A Sutton. "Systematic errors in digital image correlation caused by intensity interpolation". In: OptEn 39 (2000), pp. 2915–2921. ISSN: 0091-3286. DOI: 10.1117/1.1314593.

[43] Jacopo Baldoni et al. "Comparison of different filtering strategies to reduce noise in strain measurement with digital image correlation". In: The Journal of Strain Analysis for Engineering Design 51.6 (2016). Publisher: SAGE Publications Sage UK: London, England, pp. 416–430. ISSN: 0309-3247. DOI: 10.1177/0309324716646690.

[44] Nedaa Amraish, Andreas Reisinger, and Dieter H Pahr. "Robust Filtering Options for Higher-Order Strain Fields Generated by Digital Image Correlation". In: Applied Mechanics 1.4 (2020). Publisher: Multidisciplinary Digital Publishing Institute, pp. 174–192. DOI: 10.3390/applmech1040012.

[45] Bing Pan et al. "Full-field strain measurement using a two-dimensional Savitzky-Golay digital differentiator in digital image correlation". In: Optical Engineering 46.3 (2007). Publisher: International Society for Optics and Photonics, p. 033601. ISSN: 0091-3286. DOI: 10.1117/1.2714926.

[46] Michel Bornert et al. "Assessment of digital image correlation measurement errors: methodology and results". In: Experimental mechanics 49.3 (2009). Publisher: Springer, pp. 353–370. ISSN: 1741-2765. DOI: 10.1007/s11340-008-9204-7.

[47] Hubert Schreier, Jean Jose Orteu, and Michael A Sutton. Image correlation for shape, motion and deformation Springer Science & Business Media, 2009. ISBN: 0-387-78747-X.

[48] BD Llewellyn. "Nuclear staining with alum hematoxylin". In: Biotechnic & Histochemistry 84.4 (2009), pp. 159–177. ISSN: 1052-0295. DOI: 10.1080/10520290903052899.

[49] Cindy Sampias and Geoffrey Rolls. H&E staining overview: a g 2019. URL: https://www.leicabiosystems.com/fr-fr/knowledge-pathway/he-staining-overview-a-guide-to-best-practices/.

[50] Yves Surrel. "Les techniques optiques de mesure de champ: essai de classification". In: Instrumentation, Mesure, Métrologie 4.3-4 (2004), pp. 11–42.

[51] MA Chowdhury et al. "Friction coefficient of different material pairs under different normal loads and sliding velocities". In: Tribology in Industry 34.1 (2012). Publisher: University of Kragujevac, Faculty of Engineering, p. 18. ISSN: 0354-8996.

[52] Qiang Li et al. "Kinetics of the coefficient of friction of elastomers". In: Scientific reports 4.1 (2014). Publisher: Nature Publishing Group, pp. 1–5. ISSN: 2045-2322. DOI: 10.1038/srep05795.

[53] MW Pascoe and David Tabor. "The friction and deformation of polymers". In: Proceedings of the Royal Society of London. Series A. Mathe 235.1201 (1956). Publisher: The Royal Society London, pp. 210–224. ISSN: 0080-4630. DOI: 10.1098/rspa.1956.0077.

[54] Riadh Elleuch et al. "Surface roughness effect on friction behaviour of elastomeric material". In: Materials Science and Engineering: A 465.1-2 (2007). Publisher: Elsevier, pp. 8–12. ISSN: 0921-5093. DOI: 10.1016/j.msea.2007.02.127.

[55] Sun Yaofeng and John HL Pang. "Study of optimal subset size in digital image correlation of speckle pattern images". In: Optics and lasers in engineering 45.9 (2007). Publisher: Elsevier, pp. 967–974. ISSN: 0143-8166. DOI: 10.1016/j.optlaseng.2007.01.012.

[56] Stéphane Avril et al. "Overview of identification methods of mechanical parameters based on full-field measurements". In: Experimental Mechanics 48.4 (2008). Publisher: Springer, pp. 381–402. ISSN: 1741-2765. DOI: 10.1007/s11340-008-9148-y.

[57] Quynh Nguyen Thi Thuy. "Identification des propriétés morphologiques et hygrothermiques hétérogènes de nouveaux composites hautes performances soumis à des cycles de vieillissement thermo-hygro-mécaniques". Issue: 2013EMSE0715. Theses. Ecole Nationale Supérieure des Mines de Saint-Etienne, Oct. 2013. URL: https://tel.archives-ouvertes.fr/tel-00978753.

[58] HAMM-MING SHEU et al. "Human skin surface lipid film: an ultrastructural study and interaction with corneocytes and intercellular lipid lamellae of the stratum corneum". In: British Journal of Dermatology 140.3 (1999). Publisher: Wiley Online Library, pp. 385–391. ISSN: 0007-0963. DOI: 10.1046/j.1365-2133.1999.02697.x.

[59] Hongbo Zeng. Polymer adhesion, friction, and lubrication. John Wiley & Sons, 2013. ISBN: 978-1-118-50513-7.

[60] C Pailler-Mattei et al. "A new approach to describe the skin surface physical properties in vivo". In: Colloids and Surfaces B: Biointerfaces 68.2 (2009), pp. 200–206. ISSN: 0927-7765. DOI: 10.1016/j.colsurfb.2008.10.005.

[61] C Pailler-Mattei et al. "Contribution of stratum corneum in determining bio-tribological properties of the human skin". In: Wear 263.7-12 (2007). Publisher: Elsevier, pp. 1038–1043. ISSN: 0043-1648. DOI: 10.1016/j.wear.2007.01.128.

[62] Patrick Kékicheff. "The long-range attraction between hydrophobic macroscopic surfaces". In: Advances in colloid and interface science 270 (2019). Publisher: Elsevier, pp. 191–215. ISSN: 0001-8686. DOI: 10.1016/j.cis.2019.06.004.

[63] C Pailler-Mattei and H Zahouani. "Study of adhesion forces and mechanical properties of human skin in vivo". In: Journal of adhesion science and technology 18.15-16 (2004). Publisher: Taylor & Francis, pp. 1739–1758. ISSN: 0169-4243. DOI: 10.1163/1568561042708368.